A heuristic framework for next-generation models of geostrophic convective turbulence

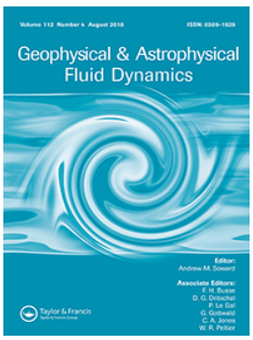

Taylor & Francis
Taylor & Francis Group

Geophysical & Astrophysical Fluid Dynamics

ISSN: 0309-1929 (Print) 1029-0419 (Online) Journal homepage: http://www.tandfonline.com/loi/ggaf20

A heuristic framework for next-generation models of geostrophic convective turbulence

Jonathan S. Cheng, Jonathan M. Aurnou, Keith Julien & Rudie P. J. Kunnen

To cite this article: Jonathan S. Cheng, Jonathan M. Aurnou, Keith Julien & Rudie P. J. Kunnen (2018) A heuristic framework for next-generation models of geostrophic convective turbulence, Geophysical & Astrophysical Fluid Dynamics, 112:4, 277-300, DOI: 10.1080/03091929.2018.1506024

To link to this article: https://doi.org/10.1080/03091929.2018.1506024

Published online: 15 Aug 2018.

GEOPHYSICAL & ASTROPHYSICAL FLUID DYNAMICS
2018, VOL. 112, NO. 4, 277–300
https://doi.org/10.1080/03091929.2018.1506024

Taylor & Francis
Taylor & Francis Group

A heuristic framework for next-generation models of geostrophic convective turbulence

Jonathan S. Cheng[a], Jonathan M. Aurnou[b], Keith Julien[c] and Rudie P. J. Kunnen[a]

[a]Turbulence and Vortex Dynamics Group, Department of Applied Physics and J.M. Burgers Center for Fluid Dynamics, Eindhoven University of Technology, Eindhoven, Netherlands; [b]Department of Earth, Planetary and Space Sciences, University of California, Los Angeles, CA, USA; [c]Department of Applied Mathematics, University of Colorado, Boulder, CO, USA

ABSTRACT

Many geophysical and astrophysical phenomena are driven by turbulent fluid dynamics, containing behaviors separated by tens of orders of magnitude in scale. While direct simulations have made large strides toward understanding geophysical systems, such models still inhabit modest ranges of the governing parameters that are difficult to extrapolate to planetary settings. The canonical problem of rotating Rayleigh-Bénard convection provides an alternate approach - isolating the fundamental physics in a reduced setting. Theoretical studies and asymptotically-reduced simulations in rotating convection have unveiled a variety of flow behaviors likely relevant to natural systems, but still inaccessible to direct simulation. In lieu of this, several new large-scale rotating convection devices have been designed to characterize such behaviors. It is essential to predict how this potential influx of new data will mesh with existing results. Surprisingly, a coherent framework of predictions for extreme rotating convection has not yet been elucidated. In this study, we combine asymptotic predictions, laboratory and numerical results, and experimental constraints to build a heuristic framework for cross-comparison between a broad range of rotating convection studies. We categorize the diverse field of existing predictions in the context of asymptotic flow regimes. We then consider the physical constraints that determine the points of intersection between flow behavior predictions and experimental accessibility. Applying this framework to several upcoming devices demonstrates that laboratory studies may soon be able to characterize geophysically-relevant flow regimes. These new data may transform our understanding of geophysical and astrophysical turbulence, and the conceptual framework developed herein should provide the theoretical infrastructure needed for meaningful discussion of these results.

ARTICLE HISTORY
Received 27 February 2018
Accepted 24 July 2018

KEYWORDS
Rotating flows; turbulent convective heat transfer; experimental methods; geophysical fluid dynamics

1. Introduction

Turbulent flows underlie many geophysical and astrophysical phenomena in the universe, from the dynamics of the oceans and atmosphere on Earth to the fluid dynamos generating magnetic fields in planets and stars (e.g. Marshall and Schott 1999, Miesch *et*

CONTACT Jonathan S. Cheng j.s.cheng@tue.nl

al. 2000, Heimpel *et al.* 2005, Roberts and King 2013). These flows are inherently difficult to investigate because their settings are too remote to allow for direct measurements. Thus, the main method for examining many such flows is to develop forward models (e.g. Busse 2000, Bahcall *et al.* 2001, Heimpel *et al.* 2005, Monchaux *et al.* 2007, Spence *et al.* 2009, Jones 2011, Soderlund *et al.* 2013). Forward models aim to capture the underlying dynamics of geophysical systems in a simplified setting. Two common methods for modelling planetary physics are to directly simulate the governing flow equations using numerical models or to investigate fluid behaviours in a laboratory setting. While direct numerical simulations (DNS) more faithfully model the overall geometry and orientation of force vectors in a geophysical system (Gastine *et al.* 2015, 2016), laboratory experiments can approach more extreme, geophysically relevant conditions (Niemela *et al.* 2000, He *et al.* 2014, Jones 2014, Aurnou *et al.* 2015, Cheng *et al.* 2015, Nataf and Schaeffer 2015).

Of the many forces involved in geophysical and astrophysical fluid processes, buoyant instabilities and rotational effects are often dominant. A reduced problem deeply relevant to these processes, then, is plane-layer thermal convection under the influence of rotation. This canonical approach takes advantage of an extensive literature of Rayleigh–Bénard convection and rotating convection studies, including theory, DNS and laboratory experiments (e.g. Malkus 1954, Rossby 1969, Julien *et al.* 1996, Grossmann and Lohse 2000, Ahlers *et al.* 2009a). Some recent numerical models take a unique approach to rotating convection by solving modified governing equations in the limit of asymptotically rapid rotation (Sprague *et al.* 2006, Julien *et al.* 2012a, 2016, Plumley *et al.* 2016). Predictions from theory and from these " asymptotically reduced" models have established that many of the behavioural regimes which are likely relevant to planetary-scale flows cannot yet be accessed by direct models of geophysical systems (Julien *et al.* 2012b, Aurnou *et al.* 2015). The simpler geometry of the rotating convection problem is better suited for reaching parameter ranges where these regimes are expected to manifest (e.g. Favier *et al.* 2014, Guervilly *et al.* 2014, Rubio *et al.* 2014, Cheng *et al.* 2015, Kunnen *et al.* 2016).

The Rayleigh number $Ra = \gamma g \Delta T H^3/(\nu\kappa)$ describes the strength of the buoyancy forcing in convection as the squared ratio between the viscous diffusion and thermal diffusion time scales, τ_ν and τ_κ, and the buoyancy forcing (free-fall) timescale $\tau_{ff} = H/U_{ff}$ squared. The convective free-fall velocity is defined here as $U_{ff} = (\gamma g \Delta T H)^{1/2}$, so $\tau_{ff} = H^{1/2}(\gamma g \Delta T)^{-1/2}$. The coefficient of thermal expansion is γ, g is the gravitational acceleration, ΔT is the adverse superadiabatic temperature gradient, H is the height of the fluid layer, ν is the kinematic viscosity and κ is the thermal diffusivity. The Prandtl number $Pr = \nu/\kappa$ gives the ratio between the thermal and viscous diffusion timescales. The Ekman number, $E = \nu/(2\Omega H^2)$ parametrises the influence of rotation as the ratio between the rotational timescale $\tau_\Omega = 1/(2\Omega)$ and the viscous time scale, where Ω is the angular rotation rate of the body. The Rossby number $Ro = U/(2\Omega H)$ also describes the influence of rotation by comparing the rotational timescale τ_Ω to the inertial timescale $\tau_i = H/U$, where U is the characteristic flow velocity. In convectively-driven flows, the buoyant free-fall timescale τ_{ff} serves as a lower bound on the inertial timescale τ_i when all heating power goes towards fluid motions (e.g. Gilman 1977, Julien *et al.* 1996, Stevens *et al.* 2009). For the limit of $\tau_i = \tau_{ff}$, a "convective Rossby number" can be defined as:

$$Ro_C = \frac{\tau_\Omega}{\tau_{ff}} = \left(\frac{\gamma g \Delta T}{(2\Omega)^2 H}\right)^{1/2} = \left(\frac{RaE^2}{Pr}\right)^{1/2}. \quad (1)$$

In geophysical settings, these parameters take on extreme values – in the Earth's outer core, for example, estimates give $Ra \sim 10^{20}$–10^{30}, $E \sim 10^{-15}$ and $Ro \sim 10^{-6}$ (Gubbins 2001, Aurnou *et al.* 2003, Schubert and Soderlund 2011). A massive separation exists between the viscous and inertial timescales, as well as between the inertial and rotational timescales ($\tau_\nu \gg \tau_i \gg \tau_\Omega$). The majority of direct simulations of the outer core, in contrast, are confined to ranges of $Ra \lesssim 10^7$, $E \gtrsim 10^{-6}$ and $Ro \gtrsim 10^{-2}$ due to numerical resolution constraints (e.g. King and Buffett 2013, Sreenivasan *et al.* 2014). Many of the behaviours expected from theory and asymptotic models may not yet manifest in these models.

While numerical models need to resolve the scale separation between different behaviours to simulate geophysically meaningful flows, laboratory experiments inherently "resolve" all of the physics, even for behaviours that are too small to detect (Roberts and King 2013). The laboratory approach is thus uniquely well suited for investigating geophysical-style rotating convection at extreme values of the governing parameters. Several new large-scale rotating convection devices have been built for this purpose (figure 1). With a potential influx of new experimental data, it is crucial to build theoretical infrastructure that fosters cross-comparison between different experiments.

In this study, we construct a predictive framework by combining asymptotic results for geostrophic convection regimes, regime transitions and heat transfer scalings detected in existing laboratory and numerical studies and physical constraints governing the accessible parameter ranges for laboratory experiments. Design considerations for optimising experiments towards exploring extreme parameter ranges are also discussed. We show that upcoming experiments may be able to reach conditions where asymptotically predicted flow behaviours manifest, allowing us to determine the relevance of such behaviours to natural phenomena.

In Section 2, we review the behavioural regimes found in theoretical studies of rotating convection as well as the heat transfer scalings and flow transitions observed so far in laboratory experiments and DNS. In Section 3, the design considerations for laboratory experiments to access and characterise these regimes are outlined. In Section 4, we discuss the rotational and heat transfer constraints needed for ensuring that the physics remains within the bounds of classical Boussinesq rotating convection. To contextualise these experimental considerations with respect to flow regime predictions, we detail the achievable parameter ranges in a collection of extreme rotating convection devices (pictured in figure 1). The significance of such laboratory experiments towards understanding geophysical systems is discussed in Section 5.

2. Flow regimes

Results from laboratory experiments, DNS and asymptotically reduced studies indicate that a variety of rotating convection flow regimes occupy the range between rotation-controlled and buoyancy-controlled convection (Julien *et al.* 2012b). To analyse the capabilities of a given experiment, we first outline these regimes and the parameter ranges over which they are expected to arise.

One method for categorising flow behaviour is to track the strength of the nondimensional heat transfer: different behaviours likely lead to different modes of heat transport,

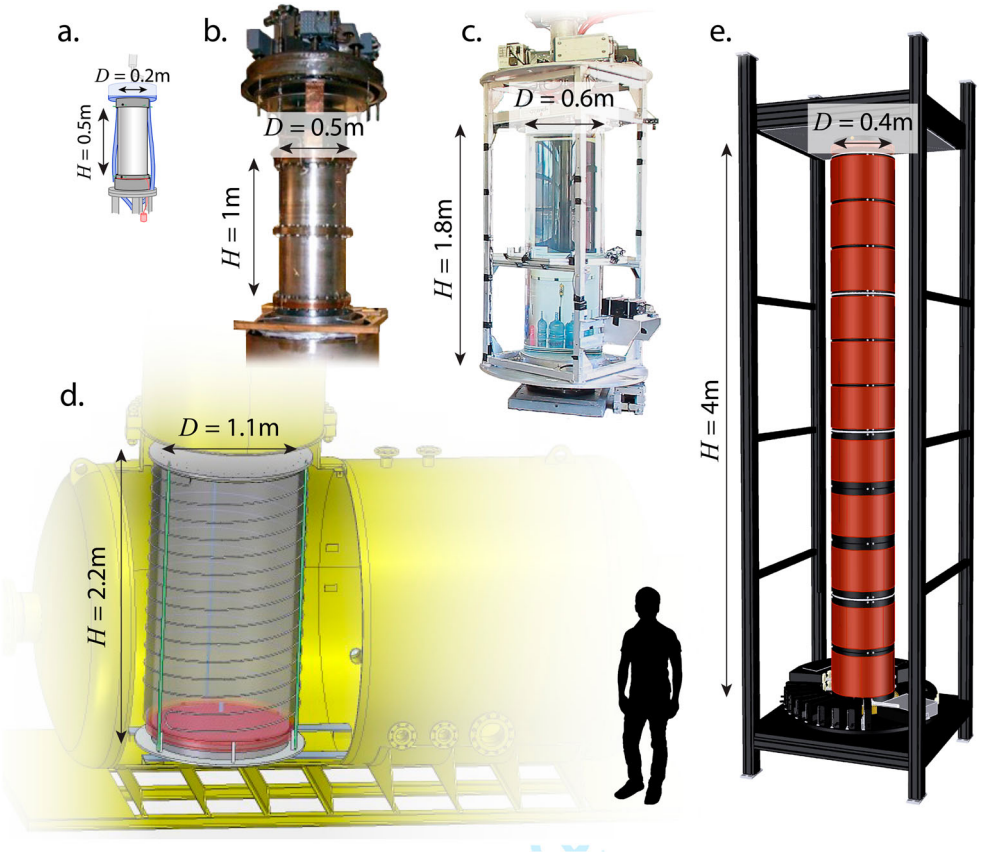

Figure 1. Images of several extreme rotating convection setups. (a) "RoMag" at UCLA (liquid gallium, $Pr \approx 0.025$) (see King and Aurnou 2013, Aurnou *et al.* 2018), (b) Trieste experiment at ICTP (cryogenic liquid He, $Pr \approx 0.7$) (see Niemela *et al.* 2000, Ecke and Niemela 2014), (c) "NoMag" at UCLA (water, $Pr \approx 4-7$), (d) "U-Boot" at the Max Planck Institute for Dynamics and Self-Organization (SF_6, N_2, He gas, $Pr \approx 0.8$) (see Ahlers *et al.* 2009b, Funfschilling *et al.* 2009) and (e) "TROCONVEX" at Eindhoven University of Technology (water, $Pr \approx 2-7$).

and thus to differences in the scaling properties (e.g. Malkus 1954, Kraichnan 1962, Castaing *et al.* 1989, Julien *et al.* 1996, Grossmann and Lohse 2000, Ahlers *et al.* 2009a). The Nusselt number $Nu = qH/(\kappa\rho C_p \Delta T)$ represents the ratio between the total heat transfer and conductive heat transfer, where C_p is the specific heat capacity and q is the heat flux per unit area (e.g. Cheng and Aurnou 2016). The governing parameters tend to be approximately related by power law scalings (e.g. Spiegel 1971); (cf. Grossmann and Lohse 2000). Here, we assume that the Nusselt number scales as

$$Nu \sim Ra^{\alpha} E^{\beta} Pr^{\delta}, \tag{2}$$

where α, β and δ are constant exponents in a given scaling regime. Fundamental behavioural transitions are associated with changes in the mode of heat transfer and therefore with changes in these scaling exponents (e.g. Julien *et al.* 2012b, Ecke and Niemela 2014, Stellmach *et al.* 2014, Cheng *et al.* 2015, Kunnen *et al.* 2016).

Figure 2 is a schematic demonstrating how Nu scales with Ra, from the onset of convection at low Ra to flows indistinguishable from nonrotating convection at high Ra (and assuming fixed E and Pr values). The flow changes morphology a number of times between these endpoints, resulting in multiple behavioural regimes. The "columnar", "plumes" and "geostrophic turbulence" regimes are derived from the asymptotic results of Julien *et al.* (2012b) and Nieves *et al.* (2014) while properties of the "nonrotating heat transfer" regime are established in classical experiments and theory (e.g. Malkus 1954, Kraichnan 1962, Spiegel 1971, Castaing *et al.* 1989). Note that between onset and $Ra/Ra_s \sim 2$, flow exists in the "cellular" regime (Veronis 1959). This regime is not marked separately on figure 2, as the heat transfer scaling does not change appreciably between this regime and the next (Julien *et al.* 2012b). We theorise that a regime of "unbalanced boundary layers" occurs beyond geostrophic turbulence but prior to the flow becoming fully insensitive to rotation. The flow behaviours of each regime are described in Appendix A.1.

The columnar regime only appears for Prandtl numbers greater than 3 (e.g. Julien *et al.* 2012b). Hence, $Pr = 3$ is used as an approximate threshold between "large" and "small" Prandtl numbers, and figure 2(a) shows the predicted regimes for $Pr > 3$ flows while 2b shows the predicted regimes for $Pr \lesssim 3$ flows. In both cases, the Nu–Ra scaling exponent α decreases as the convective forcing increases in strength relative to rotational effects. Literature predictions for α are described in Appendix A.2. Rotating convection at $Pr < 0.68$ again exhibits distinct behaviours (e.g. Chandrasekhar 1961, Horn and Schmid 2017). The main text will concern only $Pr \gtrsim 0.68$ fluids, while a discussion of $Pr < 0.68$ fluids, particularly $Pr \ll 1$ fluids such as liquid metals, is allocated to Appendix A.4.

Transition Rayleigh numbers Ra_{CP}, Ra_{PGT}, Ra_{GTU} and Ra_{UNR} separate the flow regimes in figure 2. While variations in α could function as a simple diagnostic for detecting regime transitions, most rotating convection studies find a relatively smooth transition in α between the endpoints of " rotationally dominated" convection and "buoyancy dominated" convection (e.g. Rossby 1969, King *et al.* 2012, Cheng *et al.* 2015), as shown in figure 3. It is therefore important to give predictions for where regime transitions are expected in next-generation experiments. Fortunately, the rotating convection literature contains a wide variety of theoretical predictions and experimental results for regime transitions that may apply to the asymptotic schema. We compile transitions observed in the literature in table 1 and, based on the physical arguments contained in the originating studies, we categorise them with respect to theoretically predicted regimes. The properties of each transition and rationale for their categorisation are described in more detail in Appendix A.3.

Steady, bulk convection in an infinite layer onsets at a critical Rayleigh number Ra_s in the form of overturning cells. For $Pr \gtrsim 0.68$ and $E \lesssim 10^{-3}$ (Chandrasekhar 1961) it is

$$Ra_s = 8.7E^{-4/3}. \tag{3}$$

Though Ra_s is used to indicate onset in figure 2, the topic requires further discussion: in a finite container, instabilities often first occur as drifting waves attached to the sidewall of the container rather than as bulk motions. In the asymptotic case ($E \to 0$), these "wall modes" onset at

$$Ra_w = 31.8E^{-1} \tag{4}$$

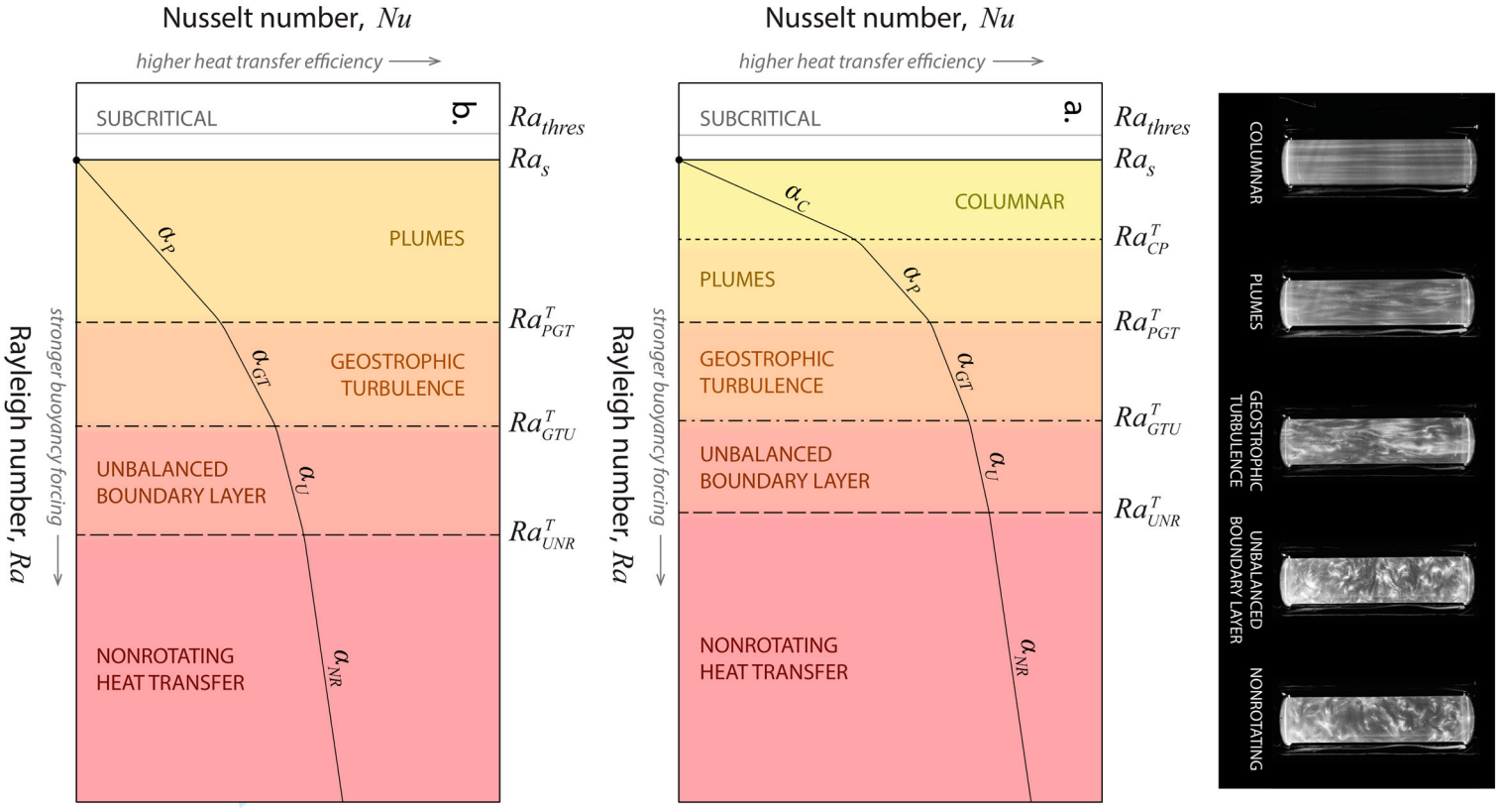

Figure 2. Schematic showing the distribution of rotating convection regimes in terms of Nusselt number (*Nu*) versus Rayleigh number (*Ra*) for a fixed Ekman number (*E*) and a) $Pr > 3$ and b) $Pr \lesssim 3$. Laboratory flow visualisations of each regime at $Pr \approx 7$, adapted from Cheng *et al.* (2015), are shown in the upper panel. In (a) and (b), the vertical lines indicate transition Rayleigh values: Ra_S denotes convective onset, Ra_{CP} denotes the transition between columnar-style convection and plumes, Ra_{PGT} between plumes and geostrophic turbulence, Ra_{GTU} between geostrophic turbulence and unbalanced boundary layers, and Ra_{UNR} to nonrotating-style convection. Though the transitions are delimited by lines, each likely occurs gradually over a range of *Ra* values. Their locations are not yet well-determined, and table 1 and figure 6 list various existing predictions. For $Pr \lesssim 3$, steady columnar convection does not occur (e.g. Julien *et al.* 2012b, Stellmach *et al.* 2014). (Colour online).

Table 1. Table showing various predictions for the transitions between different flow regimes (shown schematically in figures 2 and 4).

Transition prediction	Type	*Pr*	References	Figure abbreviation
$Ra \sim 5.4E^{-1.47}$	Ra_{CP}	≈ 7	Cheng *et al.* (2015)	Ra_{Ch15}
$Ra \sim 55E^{-4/3}$	Ra_{CP}	7	Nieves *et al.* (2014)	Ra_{Ni14}
$Ra/Ra_s \sim 3$	Ra_{PGT}	< 3	Julien *et al.* (2012a)	$Ra/Ra_s = 3$
$Ra \sim E^{-8/5}Pr^{3/5}$	Ra_{GTU}	any[a]	Julien *et al.* (2012a)	Ra_{Ju12}
$Ra \sim 1.3E^{-1.65}$	Ra_{GTU}	≈ 6	Ecke and Niemela (2014)	$Ra_{\mathrm{EN14.1}}$
$Ra \sim 0.25E^{-1.8}$	Ra_{GTU}	≈ 0.7	Ecke and Niemela (2014)	$Ra_{\mathrm{EN14.2}}$
$Ro_C \sim 0.35$	Ra_{UNR}	≈ 0.7	Ecke and Niemela (2014)	$Ro_C = 0.35$
$Ra \sim 100E^{-12/7}$	Ra_{UNR}	1	Gastine *et al.* (2016)	Ra_{Ga16}
$Ro_C \sim 1$	Ra_{UNR}	any	Gilman (1977)	$Ro_C = 1$

Notes: In the "Type" column, Ra_{CP} refers to the breakdown of well-organised convective columns into plumes, Ra_{PGT} refers to the breakdown of plumes into geostrophic turbulence, Ra_{GTU} refers to the local loss of rotational influence leading to unbalanced boundary layers and Ra_{UNR} refers to the global loss of rotational influence leading to nonrotating-style convection. The "*Pr*" column refers to the approximate Prandtl number for which the transition is observed or is predicted to apply. The "References" column gives the study from which each prediction originated. The "Figure abbreviation" column gives the label assigned to each transition in figure 6.[a]

While Julien *et al.* (2012a) did not reach the geostrophic turbulence regime for any $Pr > 3$ cases, the asymptotic argument for this transition is *Pr* independent.

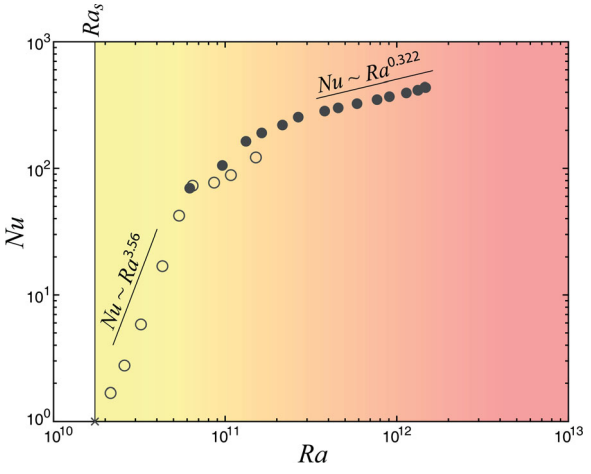

Figure 3. Example of $E \approx 10^{-7}$ rotating convection data, adapted from Cheng *et al.* (2015). Filled points correspond to laboratory experiments and open points correspond to DNS. The "×" indicates the location of steady convective onset. A steep trend of $Nu \sim Ra^{3.56}$ occurs near onset while a shallow nonrotating convection trend of $Nu \sim Ra^{0.322}$ is approached at higher *Ra* values. Between these two endpoints, no clear theoretically predicted *Nu*–*Ra* power law scalings have been detected. (Colour online).

(Herrmann and Busse 1993, Zhang and Liao 2009) with vertical and azimuthal wavenumber $= 1$ for cylindrical containers of aspect ratio $1/10 \leq \Gamma \leq 1$ (G. Vasil, private communications). Here, $\Gamma = D/H$ of the fluid layer where D is the diameter. For the sake of simplicity, we will assume going forward that Ra_s always corresponds to the onset of bulk convection (cf. Ecke 2015). It is important to note that the fluid may become unstable to wall modes as early as $Ra_w \lesssim Ra_s/100$ for some of the experiments we discuss below. Thus, we cannot discount the possibility of wall mode-induced turbulence occurring in the bulk prior to stationary onset (Horn and Schmid 2017). Though we will not address them here,

open questions abound with regard to wall modes both at very low Ekman numbers and in low Γ containers.

3. Design factors

Present-day laboratory and DNS studies are, at best, only partially able to capture the asymptotic behaviours we have catalogued above (cf. Favier *et al.* 2014, Guervilly *et al.* 2014, Stellmach *et al.* 2014). To further our understanding of extreme rotating convection, laboratory experiments must be optimised towards comparison with theory by covering broad ranges of Ra/Ra_s at extremely low values of E (e.g. $E < 10^{-7}$). Here, we discuss the physical considerations essential to designing these experiments.

Figure 4 is a schematic showing the accessible E and Ra ranges in a rotating convection setup with fixed height and width. Assuming the fluid properties are also fixed, the bounds on E are determined solely by the minimum and maximum rotation rates of the system, Ω, and the bounds on Ra are determined solely by the minimum and maximum imposed temperature difference, ΔT. The temperature difference is often imposed by applying a fixed heat flux q to the bottom boundary (e.g. Ahlers *et al.* 2009b, Ecke and Niemela 2014, Cheng *et al.* 2015), meaning the control parameter is the flux Rayleigh number

$$Ra_F = Nu \cdot Ra = \frac{\gamma g H^4 q}{\nu \kappa k}, \tag{5}$$

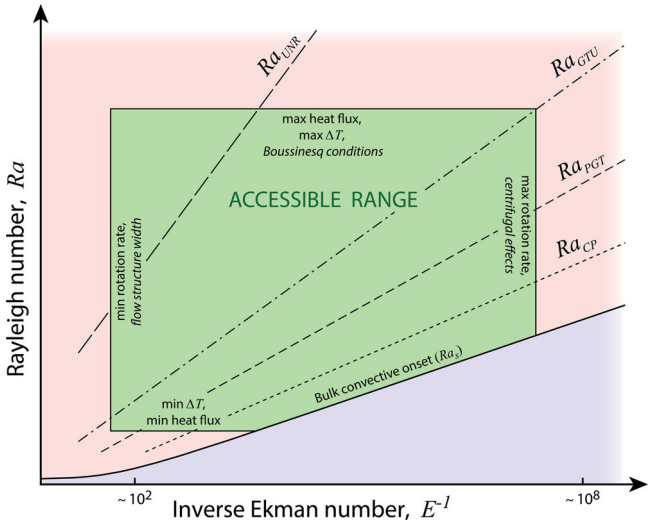

Figure 4. Schematic of accessible Ekman number, E, and Rayleigh number, Ra ranges for a given rotating convection experiment. Assuming the tank size and fluid properties are fixed, the absolute bounds on E are determined by the minimum and maximum rotation rates, Ω, and the absolute bounds on Ra are determined by the minimum and maximum temperature difference, ΔT. Minimising sidewall effects and minimising centrifugation effects require separate lower and upper bounds on Ω. Maintaining Boussinesq conditions requires a separate upper bound on ΔT. The onset of bulk convection, Ra_s is indicated by a solid black line. Different flow regimes are separated by transition Rayleigh values Ra_{CP}, Ra_{PGT}, Ra_{GTU} and Ra_{UNR} (see table 1). These transitions and the regimes they separate are difficult to distinguish at moderate-to-high E values but become distinct as E decreases. (Colour online).

where $k = \rho C_p \kappa$ is the thermal conductivity of the fluid. For a shallow Nu–Ra scaling such as $\alpha_{NR} \simeq 1/3$, $Ra \propto q^{3/4}$, while for a steep Nu–Ra scaling such as $\alpha_C \simeq 3$, $Ra \propto q^{1/4}$. In both cases, varying q is relatively inefficient for accessing broad ranges of Ra.

In contrast to the linear dependence of ΔT on Ra and Ω on E, Ra varies with H^3 and E varies with H^{-2}: changing the height of the experiment is far more effective for reaching a broad range of Ra and E values (Zhong *et al.* 1991). However, increasing the height simultaneously hinders the ability to access low values of Ra/Ra_s. The supercriticality is given by

$$\frac{Ra}{Ra_s} = \frac{Ra}{8.7E^{-4/3}} = \frac{\gamma g \nu^{1/3}}{21.9\kappa} \frac{\Delta T H^{1/3}}{\Omega^{4/3}}. \tag{6}$$

Since $Ra/Ra_s \propto H^{1/3}$, a higher tank height corresponds to a higher minimum supercriticality, thus restricting the ability to access near-onset flow regimes. To overcome this limitation, the RoMag, NoMag and TROCONVEX experiments (figure 1(a,c,d,e) use interchangeable tanks of various heights. Table 2 contains more information about these experiments. In order to completely bridge the gap between onset and the minimum achievable Ra/Ra_s in experiments, though, DNS have proven to be ideal (King *et al.* 2012, Cheng *et al.* 2015).

The U-Boot and Trieste experiments (figure 1(b,d)) can access high Ra values by taking advantage of the large ratio between thermal expansivity and the thermal and viscous diffusivites ($\gamma/\nu\kappa$) in cryogenic helium and other compressed gases (Niemela *et al.* 2000, Ahlers *et al.* 2009b, Funfschilling *et al.* 2009, Niemela *et al.* 2010). For example, at a typical operating temperature and pressure for cryogenic helium of 4.7 K and 0.12 bar, $\gamma/\nu\kappa \approx 10^{11}$ $\mathrm{s^2 m^{-4} K^{-1}}$. At a typical operating temperature of 25 °C for water, $\gamma/\nu\kappa \approx 2 \times 10^9$ $\mathrm{s^2 m^{-4} K^{-1}}$, a factor of 50 below that of helium.

Furthermore, the ability to vary the pressure allows for a greater Ra range in gas experiments. From the definition of Ra, we see that for an ideal gas:

$$Ra = \frac{\gamma g \Delta T H^3 \rho^2 C_P}{k\eta} \propto \rho^2 \propto P^2 M^2, \tag{7}$$

where η is the dynamic viscosity, P is the pressure and M is the molecular weight (Ahlers *et al.* 2009b). The quadratic relation between Ra and pressure is especially useful since the

Table 2. Design properties and constraints for the experiments shown in figure 1 and discussed in figures 5 and 6 and figure A2.

Experiment name	H (m)	D (m)	Ω (rad/s)	ΔT (°C)	Input power (W)
RoMag[1][2]	0.05, 0.1, 0.2, **0.5**	0.2	0.70†–3.1	0.4*–60*	25–5000
Trieste[3][4]	1.0	0.5	0.02–1.0*	0.03*–0.2*	0.001–20
NoMag	0.1, 0.2, 0.4, 0.8, **1.8**	0.2, **0.6**	0.05–1.8	0.4*–25*	20–1500
U-Boot[5][6]	1.1, **2.2**	1.1	0.002–1.3	1*–10.6	$\leq$ 3000
TROCONVEX	0.8, 2.0, 3.0, **4.0**	0.4	0.15–2.2	1*–25*	5–2000

Notes: For entries with multiple values, the bolded quantity is the one used in our study. We include some references for devices used in previously published results: [1] King and Aurnou (2013); [2] Aurnou *et al.* (2018); [3] Niemela *et al.* (2000); [4] Ecke and Niemela (2014); [5] Ahlers *et al.* (2009b); [6] Funfschilling *et al.* (2009). Minimum and maximum rotation rates Ω are determined by $m \geq 10$ and $Fr < 0.1$, respectively. Minimum and maximum temperature differences ΔT are determined by the measurement sensitivity and the Boussinesq limitation $\gamma \Delta T < 0.1$, respectively. An asterisk (*) in the Ω or ΔT category indicates that an experimental or diagnostic limitation is given instead because it is more restrictive than the corresponding theoretical constraint. The dagger (†) indicates that the minimum rotation rate uses an $m \geq 5$ condition instead of $m \geq 10$.

Table 3. Fluid properties for the experiments shown in figure 1 and discussed in figures 5 and 6 and figure A2.

Experiment name	Working fluid	P (bar)	T (°C)	ρ (kg/m^3)	α_T (1/K)	ν (m^2/s)	κ (m^2/s)	Pr
RoMag	Liquid Ga[1]	1	35–55	5900	1.3×10^{-4}	$(3.4 - 3.7) \times 10^{-7}$	1.3×10^{-5}	0.025–0.028
Trieste	Cryogenic He[2]	0.03–0.2	−268.5	0.3–2	0.23	$(0.54 - 3.7) \times 10^{-6}$	$(0.76 - 5.4) \times 10^{-6}$	0.69–0.72
NoMag	**Water**[3], air	1	10–50	990–1000	$(0.83 - 4.5) \times 10^{-4}$	$(0.5 - 1.3) \times 10^{-6}$	$(1.4 - 1.6) \times 10^{-7}$	3.5–9.4
U-Boot	**SF_6**[2], He, N_2	0.001–19	20–35	0.0057–160	$(3.2 - 11) \times 10^{-3}$	$1.0 \times 10^{-7} - 0.003$	$1.0 \times 10^{-7} - 0.004$	0.78–0.99
TROCONVEX	**Water**[3], air	1	20–80	970–1000	$(2 - 6) \times 10^{-4}$	$(0.34 - 1) \times 10^{-6}$	$(1.4 - 1.6) \times 10^{-7}$	2.1–6.9

Notes: In the "Working fluid" column, the bolded item is the fluid for which properties are listed. Sources for the properties are as follows: [1] Aurnou *et al.* (2018); [2] Bell *et al.* (2014); [3] Lide (2003). P gives the range of pressures used in each setup and T the range of mean temperatures. The ranges for density ρ, coefficient of thermal expansion α_T, kinematic viscosity ν, thermal diffusivity κ and Prandtl number Pr are computed for the accessible ranges of P and T in the setups.

pressure can be varied over several decades in these devices. The U-Boot device can also be filled with different gases of varying molecular weight in order to reach broader ranges of Ra and lower values of Ra/Ra_s. Table 3 lists some material properties for the fluids used in each experiment.

4. Experimental constraints

Additional limitations on the parameter coverage must be imposed to ensure that the fluid physics remains consistent with the fundamental rotating Rayleigh–Bénard convection problem (indicated by italicised text in figure 4):

- Ensuring flow structures are not overly affected by tank geometry, which constrains the minimum rotation rate
- Keeping the fluid in a Boussinesq state, which constrains the maximum imposed temperature gradient
- Minimising centrifugation effects, which constrains the maximum rotation rate

These arguments are compiled in table 4, and we use the experimental devices shown in figure 1 as examples to demonstrate the effect on accessible Ra and E ranges.

In an experimental setup, the tank geometry can affect the physics appreciably (e.g. Wu and Libchaber 1992). Many low-E numerical simulations use doubly-periodic horizontal boundary conditions with effectively no walls (cf. Julien *et al.* 2018). Limiting sidewall effects in experiments is therefore important for ensuring valid comparisons with DNS. To this end, we implement the criterion that a large number of flow structures must fit horizontally across the tank.

We define the flow structure width ratio m as:

$$m = D/\ell = c^{-1}E^{-1/3}\Gamma = c^{-1}\left(\frac{2\Omega D^3}{\nu H}\right)^{1/3}, \tag{8}$$

where $\ell = 2.4E^{1/3}$ is the typical onset width of convective rolls in $Pr \gtrsim 0.68$ fluids (see Appendix A.1). We assume that for $m \geq 10$ sidewall effects do not dominate the bulk flows

Table 4. Table cataloging upper and lower bounds on the rotation rate (Ω) and Ekman number (E), and the upper bounds on the temperature gradient (ΔT) and Rayleigh number (Ra), for cylindrical rotating convection experiments.

Condition	Dimensional constraint	Nondimensional constraint
$m \geq 10$	$\Omega_{\min} = \frac{500c^3\nu H}{D^3}$	$E_{\max} = \left(\frac{D}{10cH}\right)^3$
$Fr < 0.1$	$\Omega_{\max} = \left(\frac{0.2g}{D}\right)^{1/2}$	$E_{\min} = \left(\frac{1.25\nu^2 D}{H^4 g}\right)^{1/2}$
$\gamma\Delta T < 0.1$	$\Delta T_{\max} = \frac{0.1}{\gamma}$	$Ra_{\max} = \frac{0.1gH^3}{\nu\kappa}$

Notes: The constant prefactor $c = 2.4$. The constraints on the flow structure width ratio (m) and the Froude number (Fr) are described in (8) and (9), respectively.

in a given experiment. This choice is somewhat arbitrary: while the thickness of the sidewall boundary layer scales as $E^{1/3}$ (e.g. Greenspan and Howard 1963, Kunnen *et al.* 2013), the depth of sidewall effects on the bulk flow at low E is not well known.

Centrifugal effects contribute an upper bound on Ω, and, thus, a lower bound on E. Centrifugation is parametrised via the rotational Froude number (Homsy and Hudson 1969, Hart 2000, Curbelo *et al.* 2014):

$$Fr = \frac{\text{centrifugation}}{\text{gravity}} = \frac{\Omega^2 D}{2g}. \tag{9}$$

In the case of high Fr, the centrifugal acceleration becomes significant relative to gravitational acceleration, causing denser parcels of fluid to travel radially outward. This leads to circulation patterns that are not found in the canonical rotating convection problem (e.g. Hart 2000, Marques *et al.* 2007). To avoid the potential dynamical effects of centrifugation, we assign an upper limit of $Fr < 0.1$. Again, this choice is somewhat arbitrary: different studies have found different minimum Fr values at which centrifugation first alters the flow (cf. Koschmieder 1967, Marques *et al.* 2007, Horn and Aurnou 2018).

In figure 5, we compare the experimental device limitations to the limitations imposed by the $Fr < 0.1$, $m \geq 10$ constraints for each of the experimental setups shown in figure 1 (the imposed limitations are also summarised in table 2). Of these devices, TROCONVEX can access the lowest Ekman number at $\approx 5 \times 10^{-9}$ due to its 4 m high tallest tank. However, the device also has the thinnest aspect ratio at $\Gamma = D/H = 1/10$. For a given experiment, the accessible E range is

$$\frac{E_{\max}}{E_{\min}} = \frac{\Omega_{\max}}{\Omega_{\min}} = \frac{\left(8gFr_{\max}\right)^{1/2}}{c^3 \nu m_{\min}^3} \frac{D^{5/2}}{H}, \tag{10}$$

where $E_{\max}$, $E_{\min}$, $\Omega_{\max}$ and $\Omega_{\min}$ are defined in table 4. As shown in figure 5c, the large height and small diameter on the highest TROCONVEX tank cause its accessible E range to be relatively small ($E_{\max}/E_{\min} = 15$), while the wide diameter of the U-Boot tank ($D = 1.1$ m, $\Gamma = 1/2$) causes its accessible E range to be relatively large ($E_{\max}/E_{\min} = 780$).

Apart from the physical capabilities of the experiment, the maximum heat transfer is also restricted by the dependence of the fluid properties on the temperature. A flow is considered to follow the Boussinesq approximation – under which fluid properties do not change appreciably with temperature – when the density difference that is driving the convection is small compared to the background fluid density (Spiegel and Veronis 1960, Busse 1967, Curbelo *et al.* 2014, Horn and Shishkina 2014):

$$\frac{\Delta\rho}{\rho_0} \ll 1 \rightarrow \gamma \Delta T \ll 1, \tag{11}$$

where ρ_0 is the background density of the fluid and $\Delta\rho$ is the density perturbation. This enforces a separate upper bound on ΔT. We have chosen the condition $\gamma \Delta T = 0.1$. However, some previous experimental studies have used more relaxed conditions such as $\gamma \Delta T = 0.2$ (e.g. Niemela *et al.* 2000), while others have suggested additional criteria for ensuring Boussinesq conditions (Busse 1967, Gray and Giorgini 1976).

Figure 6 shows the accessible Ra versus E ranges for the largest tanks on rotating convection experiments. (a) TROCONVEX, (b) NoMag, (c) Trieste device and (d) U-Boot.

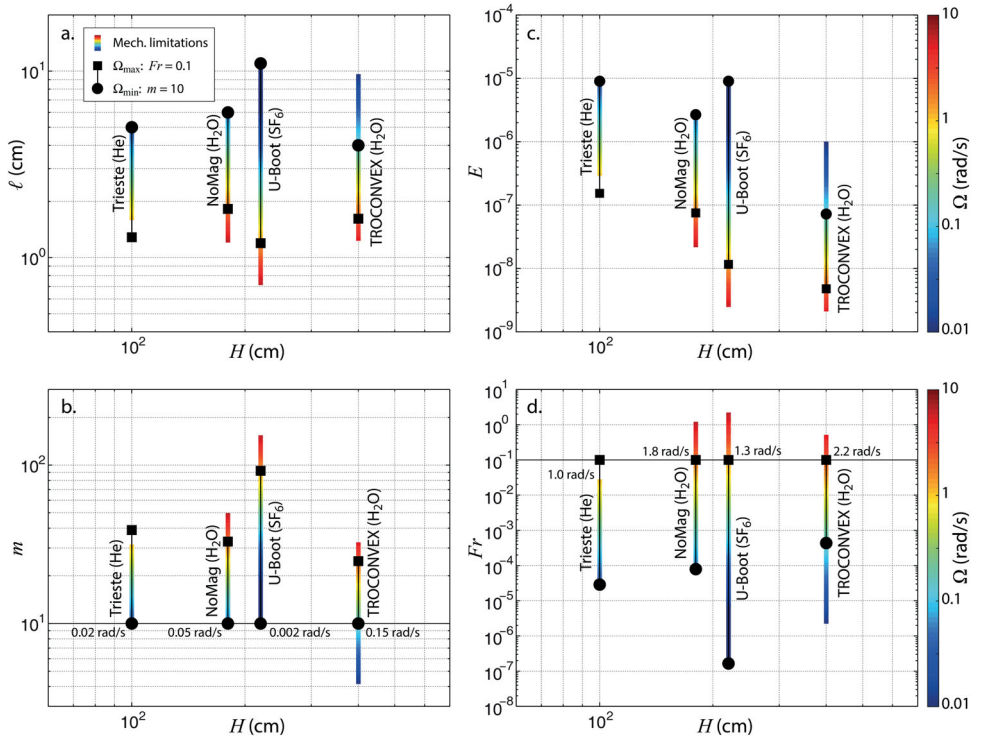

Figure 5. (a) Flow structure width ℓ, (b) flow structure width ratio m, (c) Ekman number E and (d) Froude number Fr plotted versus tank height H for four extreme rotation convection experiments. The tallest available tank in each experiment is used. The colour bars specify the minimum and maximum achievable rotation rates based on mechanical limitations of each device. The filled black square represents the maximum rotation rate Ω_{max} for which the Froude number $Fr = 0.1$, while the filled black circle represents the minimum rotation rate Ω_{min} for which the flow structure width ratio $m = 10$. The values for Ω_{min} in each experiment are given at the solid horizontal line in panel b, while the values for Ω_{max} in each experiment are given at the solid horizontal line in panel d. (Colour online).

These ranges, indicated as green boxes, are bound in E by the $m \geq 10$, $Fr < 0.1$ constraints. For the accessible Ra ranges in the water experiments (panels a and b), the $\gamma \Delta T \leq 0.1$ condition is less restrictive than experimental limitations. Instead, in both cases, the maximum ΔT is determined by the maximum applicable heat flux while the minimum ΔT is determined by the precision of the temperature measurements. The ranges of available ΔT and input power for each setup are given in table 2. Gases tend to have greater thermal expansivities and are more likely to exceed Boussinesq limitations based on (11). For example, $\Delta T < 10.6$ K is the maximum allowable temperature gradient for SF_6 in the U-Boot. These experiments are nevertheless capable of covering broad Ra ranges by also varying the pressure.

Transition predictions are given as dashed lines in figure 6. We were unable to find any formal predictions for the transition between plumes and geostrophic turbulence for $Pr > 3$ fluids, while the transition to nonrotating-style convection has several competing predictions in both $Pr > 3$ and $Pr \lesssim 3$ fluids. One topic of interest for upcoming studies is to elucidate these transitions at lower E.

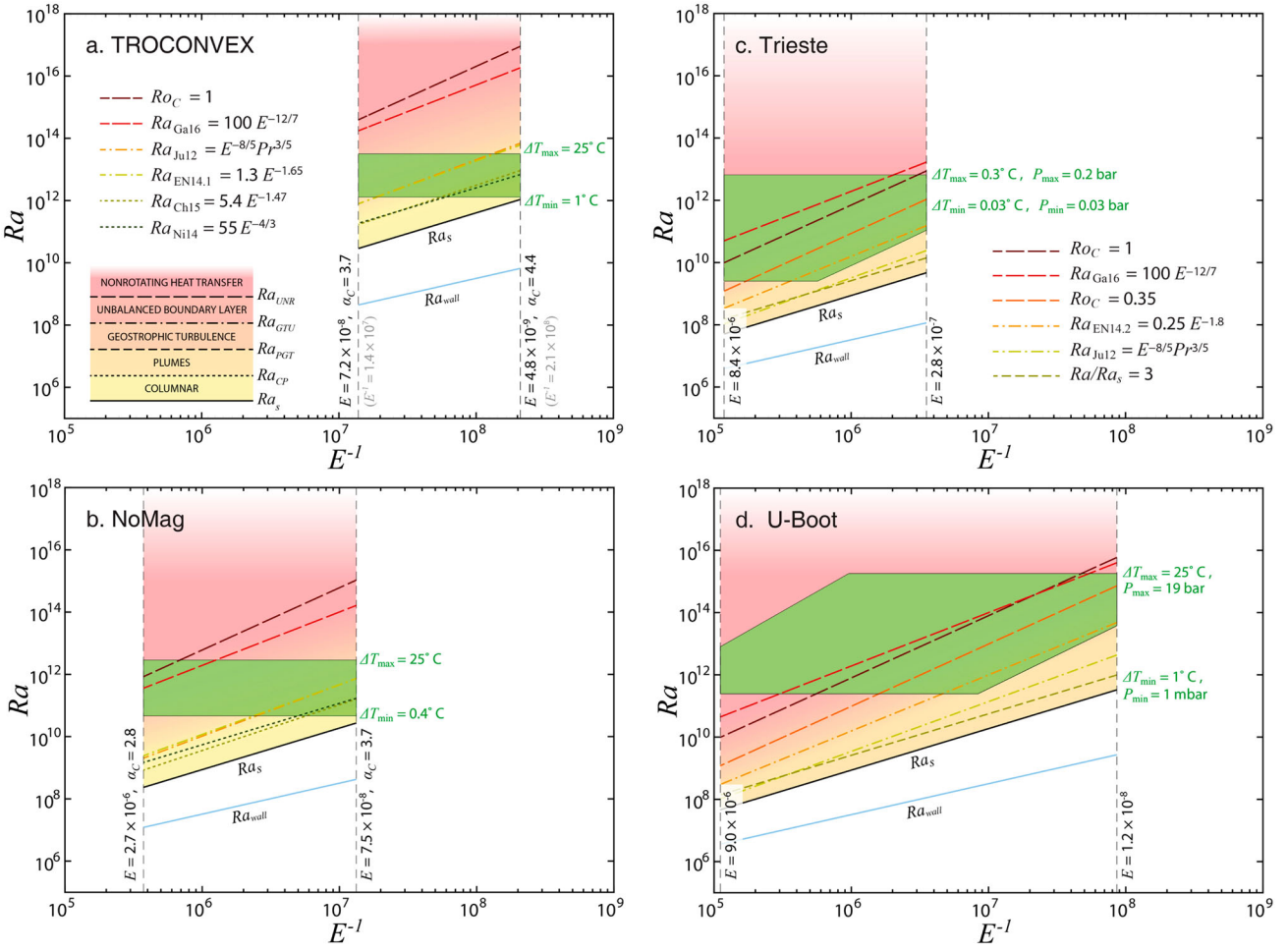

Figure 6. Rayleigh number *Ra*, plotted versus Ekman number, *E*, for the highest available tank size in each of the: (a) TROCONVEX ($Pr = 7$), (b) NoMag ($Pr = 7$), (c) Trieste ($Pr = 0.7$), and (d) U-Boot ($Pr = 0.7$) rotating convection experiments. The green box shows the range of *Ra*–*E* space accessible to each experiment assuming fixed fluid properties. At the upper and lower *E* bounds in panels a) and b), the slope of the *Nu*–*Ra* scaling expected near the onset of convection is indicated, based on the α_C trend from figure 1. Predicted regime transitions are plotted, with the line style indicating the type of transition and the line colour indicating the specific prediction (following the legend; see table 1). Different background colors depict approximate locations of different flow regimes. (colour online).

In $Pr > 3$ flows, the regime transitions between onset and nonrotating-style convection are far from evenly divided: cells, columns, plumes and geostrophic turbulence all take place relatively near onset. Both the TROCONVEX and NoMag experiments are also capable of characterising the columnar regime at low E and low Ra values (high rotation rates and low ΔT). They should comfortably access the plumes and geostrophic turbulence regimes and associated transition scalings Ra_{CP} and Ra_{PGT}, at low E ranges.

The unbalanced boundary layers regime is predicted to cover a broad Ra range for $Pr > 3$ flows, with at least two decades separating Ra_{GTU} and Ra_{UNR}. TROCONVEX and NoMag can both cover a decade of Ra in this regime, and Ra_{GTU}, though only NoMag will be able to access Ra_{UNR} and only at relatively high rotation rates and E values.

For $Pr \lesssim 3$ fluids, Ra_{GTU} may occur very close to Ra_{PGT} or be separated by a decade in Ra, depending on which prediction is relevant. The U-Boot device should be able to test the Ecke and Niemela (2014) prediction over at least a decade in E. Several competing predictions also exist for Ra_{UNR}. Both the Trieste and U-Boot experiments should be able to thoroughly test this transition, with their ability to access both the unbalanced boundary layers and nonrotating-style regimes over nearly their entire accessible E ranges and across several decades in Ra.

5. Discussion

By expanding parameter coverage, upcoming studies will create opportunities to resolve the many unknown or conflicting transition predictions, scaling relations and flow regime observations that exist in the rotating convection literature. We have compiled the key scaling predictions from multiple, independent studies to build a conceptual framework for studying the underlying physics in next-generation experiments.

Compiling results from numerous rotating convection studies reveals many gaps in our current understanding, such as a lack of predictions for the transition between plumes and geostrophic turbulence in $Pr > 3$ fluids and the existence of several competing predictions for the transition to nonrotating-style convection. Future experiments in unexplored parameter ranges will create opportunities to reconcile results from multiple, independent studies into a consistent physical model for extreme rotating convection.

Though we have outlined the regimes in terms of heat transfer, fully realising such a model will undoubtedly also require length, time and velocity scale arguments. With the appropriate diagnostics, large-scale devices are poised to address important questions concerning these scales across multiple regimes. This knowledge should, in turn, lead to better design parameters for future experiments: the relationships between length and timescales determine the types of flow structures that can develop in a tank of given dimensions (Nataf and Schaeffer 2015).

Based on existing predictions, each of the devices discussed is capable of reaching multiple behavioural regimes over broad parameter ranges. The water experiments are generally best-suited towards accessing the regimes of geostrophic turbulence and plumes and can access the columnar regime at the lower end of their accessible E ranges. The gas experiments are best suited towards accessing the unbalanced boundary layers and nonrotating convection regimes over broad E ranges. Open questions abound in every regime, and each of these devices should prove valuable for furthering our understanding of geostrophic convection.

While essential, understanding extreme geostrophic convection may only be a start towards understanding natural systems that are complicated by factors such as geometry, topographical effects, magnetic forces, compositional gradients, etc. Despite the complexity of these flows, though, there is evidence that purely hydrodynamic behaviours give critical insight into natural phenomena (e.g. Käpylä *et al.* 2011, Aurnou *et al.* 2015). As experiments foray into increasingly extreme conditions, they have a greater chance of encountering behaviours that are intimately linked to geophysics. The converse is also true: behaviours at moderate parameters which seem to underly natural phenomena can fail to scale up to more geophysical parameters (Aurnou *et al.* 2015, Cheng *et al.* 2015). In either case, laboratory studies are needed to form a concrete understanding of extreme flows in a real-world setting. Developments in rotating convection are already bridging the gap between small-scale models and planetary-scale systems. Further advancing our understanding of rotating convection will require insights gained from both the current suite of experiments and from future experimental endeavours.

Acknowledgments

The authors thank Joseph Niemela and Robert Ecke for providing information about and images of the Trieste rotating convection experiment, and Ladislav Skrbek for providing the means to calculate the fluid properties of cryogenic helium. The authors also thank Stephan Weiss and Dennis van Gils for providing information and a schematic for the U-Boot device.

Disclosure statement

No potential conflict of interest was reported by the authors.

Funding

J. S. C. and R. P. J. K. have received funding from the H2020 European Research Council (ERC) under the European Union's Horizon 2020 research and innovation programme [grant number 678634]. J. M. A. and K. J. thank the NSF Geophysics program for the financial support.

References

Ahlers, G., Grossman, S. and Lohse, D., Heat transfer and large scale dynamics in turbulent Rayleigh-Bénard convection. *Rev. Mod. Phys.* 2009a, **81**, 503–537.

Ahlers, G., Funfschilling, D. and Bodenschatz, E., Transitions in heat transport by turbulent convection at Rayleigh numbers up to 10^{15}. *New J. Phys.* 2009b, **11**, 123001.

Aurnou, J.M., Andreadis, S., Zhu, L. and Olson, P.L., Experiments on convection in Earth's core tangent cylinder. *Earth Planet. Sci. Lett.* 2003, **212**, 119–134.

Aurnou, J.M., Heimpel, M.H. and Wicht, J., The effects of vigorous mixing in a convective model of zonal flow on the ice giants. *Icarus* 2007, **190**, 110–126.

Aurnou, J.M., Calkins, M.A., Cheng, J.S., Julien, K., King, E.M., Nieves, D., Soderlund, K.M. and Stellmach, S., Rotating convective turbulence in Earth and planetary cores. *Phys. Earth Planet. Inter.* 2015, **246**, 52–71.

Aurnou, J.M., Bertin, V., Grannan, A.M., Horn, S. and Vogt, T., Rotating thermal convection in liquid gallium: Multi-modal flow, absent steady columns. *J. Fluid Mech.* 2018, **846**, 846–876.

Bahcall, J.N., Pinsonneault, M.H. and Basu, S., Solar models: Current epoch and time dependences, neutrinos, and helioseismological properties. *Astrophys. J.* 2001, **555**, 990.

Bell, I.H., Wronski, J., Quoilin, S. and Lemort, V., Pure and pseudo-pure fluid thermophysical property evaluation and the open-source thermophysical property library CoolProp. *Ind. Eng. Chem. Res.* 2014, **53**, 2498–2508.
Busse, F.H., The stability of finite amplitude cellular convection and its relation to an extremum principle. *J. Fluid Mech.* 1967, **30**, 625–649.
Busse, F.H., Homogeneous dynamos in planetary cores and in the laboratory. *Ann. Rev. Fluid Mech.* 2000, **32**, 383–408.
Castaing, B., Gunaratne, G., Heslot, F., Kadanoff, L., Libchaber, A., Thomae, S., Wu, X.Z., Zaleski, S. and Zanetti, G., Scaling of hard thermal turbulence in Rayleigh-Benard convection. *J. Fluid Mech.* 1989, **204**, 1–30.
Chandrasekhar, S., *Hydrodynamic and Hydromagnetic Stability*, 1st edn, 1961. Oxford, UK (Oxford University Press).
Chavanne, X., Chilla, F., Chabaud, B., Castaing, B. and Hébral, B., Turbulent Rayleigh–Bénard convection in gaseous and liquid He. *Phys. Fluids* 2001, **13**, 1300–1320.
Cheng, J.S. and Aurnou, J.M., Tests of diffusion-free scaling behaviors in numerical dynamo datasets. *Earth Planet. Sci. Lett.* 2016, **436**, 121–129.
Cheng, J.S., Stellmach, S., Ribeiro, A., Grannan, A., King, E.M. and Aurnou, J.M., Laboratory-numerical models of rapidly rotating convection in planetary cores. *Geophys. J. Int.* 2015, **201**, 1–17.
Chillá, F., Ciliberto, S., Innocenti, C. and Pampaloni, E., Boundary layer and scaling properties in turbulent thermal convection. *Il Nuovo Cimento D.* 1993, **15**, 1229–1249.
Christensen, U.R. and Aubert, J., Scaling properties of convection-driven dynamos in rotating spherical shells and application to planetary magnetic fields. *Geophys. J. Int.* 2006, **166**, 97–114.
Cioni, S., Ciliberto, S. and Sommeria, J., Strongly turbulent Rayleigh-Bénard convection in mercury: Comparison with results at moderate Prandtl number. *J. Fluid Mech.* 1987, **335**, 111–140.
Curbelo, J., Lopez, J.M., Mancho, A.M. and Marques, F., Confined rotating convection with large Prandtl number: Centrifugal effects on wall modes. *Phys. Rev. E* 2014, **89**, 013019.
Ecke, R.E., Scaling of heat transport near onset in rapidly rotating convection. *Phys. Lett. A* 2015, **379**, 2221–2223.
Ecke, R.E. and Niemela, J.J., Heat transport in the geostrophic regime of rotating Rayleigh-Bénard convection. *Phys. Rev. Lett.* 2014, **113**, 114301.
Favier, B., Silvers, L.J. and Proctor, M.R.E., Inverse cascade and symmetry breaking in rapidly rotating Boussinesq convection. *Phys. Fluids* 2014, **26**, 096605.
Funfschilling, D., Brown, E., Nikolaenko, A. and Ahlers, G., Heat transport by turbulent Rayleigh-Bénard convection in cylindrical samples with aspect ratio one and larger. *J. Fluid Mech.* 2005, **536**, 145–154.
Funfschilling, D., Bodenschatz, E. and Ahlers, G., Search for the 'ultimate state' in turbulent Rayleigh-Bénard convection. *Phys. Rev. Lett.* 2009, **103**, 014503.
Gastine, T., Yadav, R.K., Morin, J., Reiners, A. and Wicht, J., From solar-like to antisolar differential rotation in cool stars. *MNRAS Lett.* 2014, **438**, L76–L80.
Gastine, T., Wicht, J. and Aurnou, J.M., Turbulent Rayleigh-Bénard convection in spherical shells. *J. Fluid Mech.* 2015, **778**, 721–764.
Gastine, T., Wicht, J. and Aubert, J., Scaling regimes in spherical shell rotating convection. *J. Fluid Mech.* 2016, **808**, 690–732.
Gilman, P.A., Nonlinear dynamics of Boussinesq convection in a deep rotating spherical shell-I. *Geophys. Astrophys. Fluid Dyn.* 1977, **8**, 93–135.
Glazier, J.A., Segawa, T., Naert, A. and Sano, M., Evidence against 'ultrahard' thermal turbulence at very high Rayleigh numbers. *Nature* 1999, **398**, 307–310.
Gray, D.D. and Giorgini, A., The validity of the Boussinesq approximation for liquids and gases. *Int. J. Heat Mass Transfer* 1976, **19**, 545–551.
Greenspan, H.P. and Howard, L.N., On a time-dependent motion of a rotating fluid. *J. Fluid Mech.* 1963, **17**, 385–404.

Grooms, I., Julien, K., Weiss, J.B. and Knobloch, E., Model of convective Taylor columns in rotating Rayleigh-Bénard convection. *Phys. Rev. Lett.* 2010, **104**, 224501.
Grossmann, S. and Lohse, D., Scaling in thermal convection: A unifying theory. *J. Fluid Mech.* 2000, **407**, 27–56.
Gubbins, D., The Rayleigh number for convection the Earth's core. *Phys. Earth Planet. Inter.* 2001, **128**, 3–12.
Guervilly, C., Hughes, D.W. and Jones, C.A., Large-scale vortices in rapidly rotating Rayleigh-Bénard convection. *J. Fluid Mech.* 2014, **758**, 407–435.
Hart, J.E., On the influence of centrifugal buoyancy on rotating convection. *J. Fluid Mech.* 2000, **403**, 133–151.
He, X., Funfschilling, D., Nobach, H., Bodenschatz, E. and Ahlers, G., Transition to the ultimate state of turbulent Rayleigh-Bénard convection. *Phys. Rev. Lett.* 2012, **108**, 024502.
He, X., Shang, X.D. and Tong, P., Test of the anomalous scaling of passive temperature fluctuations in turbulent Rayleigh-Bénard convection with spatial inhomogeneity. *J. Fluid Mech.* 2014, **753**, 104–130.
Heard, W.B. and Veronis, G., Asymptotic treatment of the stability of a rotating layer of fluid with rigid boundaries. *Geophys. Fluid Dyn.* 1971, **2**, 299–316.
Heimpel, M., Aurnou, J. and Wicht, J., Simulation of equatorial and high-latitude jets on Jupiter in a deep convection model. *Nature* 2005, **438**, 193–196.
Herrmann, J. and Busse, F.H., Asymptotic theory of wall-attached convection in a rotating fluid layer. *J. Fluid Mech.* 1993, **255**, 183–194.
Homsy, G.M. and Hudson, J.L., Centrifugally driven thermal convection in a rotating cylinder. *J. Fluid Mech.* 1969, **35**, 33–52.
Horanyi, S., Krebs, L. and Müller, U., Turbulent Rayleigh-Bénard convection in low Prandtl number fluids. *Int. J. Heat Mass Transfer* 1999, **42**, 3983–4003.
Horn, S. and Aurnou, J.M., Regimes of Coriolis-centrifugal convection. *Phys. Rev. Lett.* 2018, **120**, 204502.
Horn, S. and Schmid, P.J., Prograde, retrograde, and oscillatory modes in rotating Rayleigh-Bénard convection. *J. Fluid Mech.* 2017, **831**, 182–211.
Horn, S. and Shishkina, O., Rotating non-Oberbeck-Boussinesq Rayleigh-Bénard convection in water. *Phys. Fluids* 2014, **26**, 055111.
Jones, C.A., Planetary magnetic fields and fluid dynamos. *Ann. Rev. Fluid Mech.* 2011, **43**, 583–614.
Jones, C.A., A dynamo model of Jupiter's magnetic field. *Icarus* 2014, **241**, 148–159.
Jones, C.A., Moore, D.R. and Weiss, N.O., Axisymmetric convection in a cylinder. *J. Fluid Mech.* 1976, **73**, 353–388.
Julien, K. and Knobloch, E., Strongly nonlinear convection cells in a rapidly rotating fluid layer: The tilted f-plane. *J. Fluid Mech.* 1998, **360**, 141–178.
Julien, K., Legg, S., McWilliams, J. and Werne, J., Rapidly rotating turbulent Rayleigh-Bénard convection. *J. Fluid Mech.* 1996, **322**, 243–273.
Julien, K., Knobloch, E., Rubio, A.M. and Vasil, G.M., Heat transport in low-Rossby-number Rayleigh-Bénard convection. *Phys. Rev. Lett.* 2012a, **109**, 254503.
Julien, K., Rubio, A.M., Grooms, I. and Knobloch, E., Statistical and physical balances in low Rossby number Rayleigh-Bénard convection. *Geophys. Astrophys. Fluid Dyn.* 2012b, **106**, 254503.
Julien, K., Aurnou, J.M., Calkins, M.A., Knobloch, E., Marti, P., Stellmach, S. and Vasil, G.M., A nonlinear model for rotationally constrained convection with Ekman pumping. *J. Fluid Mech.* 2016, **798**, 50–87.
Julien, K., Knobloch, E. and Plumley, M., Impact of domain anisotropy on the inverse cascade in geostrophic turbulent convection. *J. Fluid Mech.* 2018, **837**, R4.
Käpylä, P.J., Korpi, M.J. and Hackman, T., Starspots due to large-scale vortices in rotating turbulent convection. *Astrophys. J.* 2011, **742**, 34–41.
King, E.M. and Aurnou, J.M., Thermal evidence for Taylor columns in turbulent rotating Rayleigh-Bénard convection. *Phys. Rev. E* 2012, **85**, 016313.

King, E.M. and Aurnou, J.M., Turbulent convection in liquid metal with and without rotation. *Proc. Natl. Acad. Sci. USA* 2013, **110**, 6688–6693.
King, E.M. and Buffett, B.A., Flow speeds and length scales in geodynamo models: The role of viscosity. *Earth Planet. Sci. Lett.* 2013, **371**, 156–162.
King, E.M., Stellmach, S. and Aurnou, J.M., Heat transfer by rapidly rotating Rayleigh-Bénard convection. *J. Fluid Mech.* 2012, **691**, 568–582.
Koschmieder, E.L., On convection on a uniformly heated rotating plane. *Beitr. Phys. Atmos.* 1967, **40**, 216–225.
Kraichnan, R.H., Turbulent thermal convection at arbitrary Prandtl number. *Phys. Fluids* 1962, **5**, 1374–1389.
Kunnen, R.P.J., Clercx, H.J.H. and Geurts, B.J., Breakdown of large-scale circulation in turbulent rotating convection. *EPL (Europhys. Lett.)* 2008, **84**, 24001.
Kunnen, R.P.J., Clercx, H.J.H. and van Heijst, G.J.F., The structure of sidewall boundary layers in confined rotating Rayleigh-Bénard convection. *J. Fluid Mech.* 2013, **727**, 509–532.
Kunnen, R.P.J., Ostilla-Mónico, R., van der Poel, E.P., Verzicco, R. and Lohse, D., Transition to geostrophic convection: The role of the boundary conditions. *J. Fluid Mech.* 2016, **799**, 413–432.
Lide, D.R., *CRC Handbook of Chemistry and Physics: A Ready–Reference Book of Chemical and Physical Data: 2003–2004*, 2003. Florida, USA (CRC Press).
Malkus, W.V., The heat transport and spectrum of thermal turbulence. *Proc. Roy. Soc. Lond. A* 1954, **225**, 196–212.
Marques, F., Mercader, I., Batiste, O. and Lopez, J.M., Centrifugal effects in rotating convection: axisymmetric states and three-dimensional instabilities. *J. Fluid Mech.* 2007, **580**, 303–318.
Marshall, J. and Schott, F., Open-ocean convection: Observations, theory, and models. *Rev. Geophys.* 1999, **37**, 1–64.
Miesch, M.S., Elliott, J.R., Toomre, J., Clune, T.L., Glatzmaier, G.A. and Gilman, P.A., Three-dimensional spherical simulations of solar convection. I. Differential rotation and pattern evolution achieved with laminar and turbulent states. *Astrophys. J.* 2000, **532**, 593.
Monchaux, R., Berhanu, M., Bourgoin, M., Moulin, M., Odier, P., Pinton, J.F., Volk, R., Fauve, S., Mordant, N., Pétrélis, F., Chiffaudel, A., Daviaud, F., Dubrulle, B., Gasquet, C., Marié, L. and Ravelet, F., Generation of a magnetic field by dynamo action in a turbulent flow of liquid sodium. *Phys. Rev. Lett.* 2007, **98**, 044502.
Nataf, H.C. and Schaeffer, N.. Turbulence in the Core. In *Treatise on Geophysics*, 2nd edn, Vol. 8, pp. 161–181, 2015 (Elsevier: Oxford).
Niemela, J.J., Skrbek, L., Sreenivasan, K.R. and Donnelly, R.J., Turbulent convection at very high Rayleigh numbers. *Nature* 2000, **404**, 837–840.
Niemela, J.J., Babuin, S. and Sreenivasan, K.R., Turbulent rotating convection at high Rayleigh and Taylor numbers. *J. Fluid Mech.* 2010, **649**, 509–522.
Nieves, D., Rubio, A.M. and Julien, K., Statistical classification of flow morphology in rapidly rotating Rayleigh-Bénard convection. *Phys. Fluids* 2014, **26**, 086602.
Plumley, M., Julien, K., Marti, P. and Stellmach, S., The effects of Ekman pumping on quasi-geostrophic Rayleigh-Bénard convection. *J. Fluid Mech.* 2016, **803**, 51–71.
Roberts, P.H. and King, E.M., On the genesis of the Earth's magnetism. *Rev. Prog. Phys.* 2013, **76**, 096801.
Rossby, H.T., A study of Bénard convection with and without rotation. *J. Fluid Mech.* 1969, **36**, 309–335.
Rubio, A.M., Julien, K., Knobloch, E. and Weiss, J.B., Upscale energy transfer in three-dimensional rapidly rotating turbulent convection. *Phys. Rev. Lett.* 2014, **112**, 144501.
Scheel, J.D. and Schumacher, J., Global and local statistics in turbulent convection at low Prandtl numbers. *J. Fluid Mech.* 2016, **802**, 147–173.
Schubert, G. and Soderlund, K.M., Planetary magnetic fields: Observations and models. *Phys. Earth Planet. Inter.* 2011, **187**, 92–108.
Schumacher, J., Götzfried, P. and Scheel, J.D., Enhanced enstrophy generation for turbulent convection in low-Prandtl-number fluids. *Proc. Natl. Acad. Sci. USA* 2015, **112**, 9530–9535.

Shraiman, B.I. and Siggia, E.D., Heat transport in high Rayleigh-number convection. *Phys. Rev. A* 1990, **42**, 3650.
Soderlund, K.M., Heimpel, M.H., King, E.M. and Aurnou, J.M., Turbulent models of ice giant internal dynamics: Dynamos, heat transfer, and zonal flows. *Icarus* 2013, **224**, 97–113.
Spence, E.J., Reuter, K. and Forest, C.B., A spherical plasma dynamo experiment. *Astrophys. J.* 2009, **700**, 470.
Spiegel, E., Convection in stars. I. Basic Boussinesq convection. *Annu. Rev. Astron. Astrophys.* 1971, **9**, 323–352.
Spiegel, E.A. and Veronis, G., On the Boussinesq approximation for a compressible fluid. *Astrophys. J.* 1960, **131**, 442.
Sprague, M., Julien, K., Knobloch, E. and Werne, J., Numerical simulation of an asymptotically reduced system for rotationally constrained convection. *J. Fluid Mech.* 2006, **551**, 141–174.
Sreenivasan, B., Sahoo, S. and Dhama, G., The role of buoyancy in polarity reversals of the geodynamo. *Geophys. J. Int.* 2014, **199**, 1698–1708.
Stellmach, S. and Hansen, U., Cartesian convection driven dynamos at low Ekman number. *Phys. Rev. E* 2004, **70**, 056312.
Stellmach, S., Lischper, M., Julien, K., Vasil, G., Cheng, J.S., Ribeiro, A., King, E.M. and Aurnou, J.M., Approaching the asymptotic regime of rapidly rotating convection: Boundary layers versus interior dynamics. *Phys. Rev. Lett.* 2014, **113**, 254501.
Stevens, R.J.A.M., Zhong, J.Q., Clercx, H.J.H., Ahlers, G. and Lohse, D., Transitions between turbulent states in rotating Rayleigh-Bénard convection. *Phys. Rev. Lett.* 2009, **103**, 024503.
Veronis, G., Cellular convection with finite amplitude in a rotating fluid. *J. Fluid Mech.* 1959, **5**, 401–435.
Weiss, S. and Ahlers, G., Heat transport by turbulent rotating Rayleigh-Bénard convection and its dependence on the aspect ratio. *J. Fluid Mech.* 2011, **684**, 407–426.
Wu, X.Z. and Libchaber, A., Scaling relations in thermal turbulence: The aspect-ratio dependence. *Phys. Rev. A* 1992, **45**, 842.
Zhang, K. and Liao, X., The onset of convection in rotating circular cylinders with experimental boundary conditions. *J. Fluid Mech.* 2009, **622**, 63–73.
Zhang, K. and Schubert, G., Magnetohydrodynamics in rapidly rotating spherical systems. *Ann. Rev. Fluid Mech.* 2000, **32**, 409–443.
Zhong, F., Ecke, R.E. and Steinberg, V., Asymmetric modes and the transition to vortex structures in rotating Rayleigh-Bénard convection. *Phys. Rev. Lett.* 1991, **67**, 2473.

Appendix 1. Rotating convection regimes, scalings, and transitions

A.1 Regime predictions

Between onset and $Ra/Ra_s \sim 2$, flow exists in the cellular regime (Veronis 1959) (this regime is not marked separately on figure 2, as the heat transfer scaling does not change appreciably between this regime and the next (Julien *et al.* 2012b)). For $Pr > 3$, as Ra/Ra_s increases, the "columnar" regime manifests (Sprague *et al.* 2006, Grooms *et al.* 2010). The bulk flow in this regime is dominated by quasi-steady convective Taylor columns, created by synchronisation of the plumes emitting from the top and bottom boundary layers, and consisting of vortex cores surrounded by a shield of oppositely signed vorticity (Julien *et al.* 2012b). In both the cellular and convective Taylor column regimes, the geostrophic balance between the Coriolis force and the pressure gradient is perturbed by viscous effects. This leads to narrow structures with a horizontal length scale of (e.g. Zhang and Schubert 2000, Stellmach and Hansen 2004):

$$\ell = cE^{1/3}H = c\left(\frac{\nu H}{2\Omega}\right)^{1/3}, \tag{A.1}$$

where c is a prefactor. While Chandrasekhar (1961) derives an asymptotic value of $c = 4.8$ for the infinite plane layer, we use $c = 2.4$ instead to account for the effects of Ekman pumping at $E > 10^{-7}$

(Heard and Veronis 1971, Julien *et al.* 2016). For $Pr \lesssim 3$ the steady columnar regime is not expected to manifest (e.g. Julien *et al.* 2012b, King and Aurnou 2013).

At $Pr > 3$ and Rayleigh numbers in the vicinity of Ra_{CP} (marked by the short dashed lines in figure 2), the shields surrounding the vortex cores in the columnar regime deteriorate and the flow enters the "plumes" regime. For $Pr \lesssim 3$, this regime develops directly out of cellular convection. The rising and falling plumes ejected from the boundaries are exposed to strong vortex–vortex interactions due to the deterioration of their shields, preventing them from synchronising. This leads to structures which share the same horizontal length scale as columns and cells but which do not extend across the entire fluid layer (Julien *et al.* 2012b).

Around Ra_{PGT}, shown as medium dashed lines in figure 2, the "geostrophic turbulence" regime manifests. The plumes become confined close to the thermal boundary layers and the bulk of the fluid becomes dominated by strong mixing and vortex–vortex interactions (Julien *et al.* 2012b). Though small-scale turbulence is present, geostrophy still persists as the primary force balance and still imparts an effective vertical stiffness to the flow field.

Around Ra_{GTU}, shown as dot dashed lines in figure 2, geostrophy in the thermal boundary layers breaks down, leading to the theorised "unbalanced boundary layer" regime. The flow morphology here is not well-understood for $E \lesssim 10^{-7}$, and should be the subject of future studies.

Finally, around Rayleigh number Ra_{UNR}, shown as long-dashed lines in figure 2, the "nonrotating-style heat transfer" regime is established as the flow field becomes effectively insensitive to Coriolis forces. For large enough Ra, the bulk of the fluid becomes nearly isothermal and the temperature gradients are almost entirely confined to the boundary layers.

A.2 Heat transfer scaling (α) predictions

As Ra/Ra_s increases from onset for fixed E, decreasing rotational control allows lateral mixing in the flow to increase. This causes Nu to scale more weakly with Ra in each subsequent regime at higher Ra/Ra_s. Here we will overview the Nu–Ra scaling trends detected in previous rotating convection studies.

In the columnar regime, the heat transfer follows steep $Nu \propto Ra^{\alpha_C}$ trends, with $\alpha_C \gtrsim 3$ for $E \lesssim 10^{-6}$ (King *et al.* 2012, Stellmach *et al.* 2014, Cheng *et al.* 2015). The steepness of this trend is due to Ekman pumping effects, which greatly boost the heat transfer for a given thermal forcing (Stellmach *et al.* 2014, Kunnen *et al.* 2016). Julien *et al.* (2016) theorise that Ekman pumping effects kick in above a threshold Rayleigh number

$$Ra_{EP} \sim E^{-13/9}. \tag{A.2}$$

This scaling implies that Ekman pumping should affect the flow immediately upon the onset of bulk convection for $E \gtrsim 10^{-9}$, although it is not known what the prefactor is for experiments. If we assume a prefactor of unity, then Ra_{EP} lies below stationary onset Ra_s for all of the experimental setups discussed.

Figure A1 demonstrates that the α_C scaling exponent continues to steepen as E decreases in $Pr \simeq 7$ laboratory and numerical rotating convection data from (Cheng *et al.* 2015). The best-fit trend is given by

$$\alpha_C = -0.45 - 0.59 \log E. \tag{A.3}$$

In asymptotically reduced simulations with parametrised Ekman pumping, Plumley *et al.* (2016) find steep α_C trends at $E = 10^{-7}$, in agreement with laboratory and numerical results. As experiments become capable of reaching more extreme E ranges, they will test whether the columnar Nu–Ra scaling evolves in a manner similar to asymptotic cases.

In the geostrophic turbulence regime, Julien *et al.* (2012a) argue that the heat transport law should be independent of dissipation and predict that $Nu \sim Ra^{3/2}E^2Pr^{-1/2}$ ($\alpha_{GT} = 3/2$) (cf. Christensen and Aubert 2006). This is corroborated by Gastine *et al.* (2016), whose $Pr = 1$ spherical shell rotating convection data follow a $Nu \sim Ra^{3/2}$ scaling for $Ra > 0.4E^{-8/5}$.

In the nonrotating-style heat transfer regime, a variety of Ra- and Pr-dependent predictions exist for α_{NR} (Grossmann and Lohse 2000, Ahlers *et al.* 2009a). At high enough Ra, the temperature gradient becomes confined to the boundary layers. The heat transfer then becomes independent of the

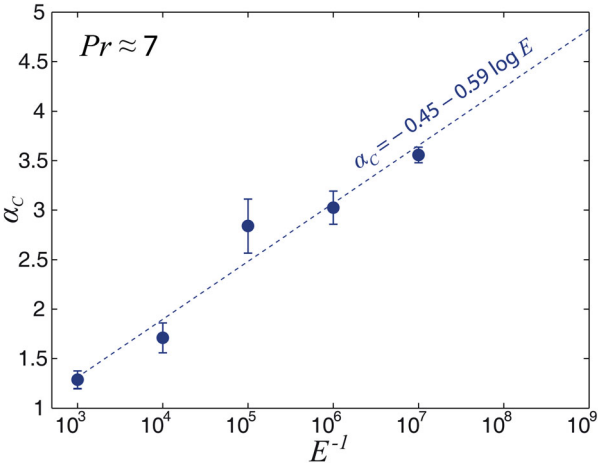

Figure A1. Slope of Nusselt number versus Rayleigh number scaling in the columnar regime, α_C, plotted versus Ekman number, E, for $Pr \simeq 7$ laboratory-numerical rotating convection data from Cheng *et al.* (2015). The dashed line shows the best-fit slope between α_C and E. (colour online).

total height, leading to $\alpha_{NR} = 1/3$ (Malkus 1954). Water experiments have found evidence for this regime at $Ra \gtrsim 10^{10}$ (Funfschilling *et al.* 2005, Cheng *et al.* 2015). At even higher Ra values, Kraichnan (1962) and Spiegel (1971) predict that the boundary layers should become fully turbulent and the heat transfer should become independent of the diffusivities, leading to $\alpha_{NR} = 1/2$ (with logarithmic corrections). Some experiments find an increase in the heat transfer scaling at high Ra (Chavanne *et al.* 2001, He *et al.* 2012), though this result is not universally supported (Niemela *et al.* 2000). The majority of studies at $Ra < 10^{10}$ and $Pr \gtrsim 1$ instead find $\alpha_{NR} \approx 2/7$ (Rossby 1969, Chillá *et al.* 1993, Glazier *et al.* 1999), theorised to be a nonasymptotic modification to the $\alpha_{NR} = 1/3$ scaling (e.g. Castaing *et al.* 1989, Shraiman and Siggia 1990). However, estimates of Ra for planetary and stellar systems place them well beyond the expected parameter range for which the $\alpha_{NR} = 2/7$ scaling remains valid (e.g. Schubert and Soderlund 2011).

In summary, a wealth of heat transfer scaling predictions exist for nonrotating and rotating convection. The relevance of each scaling to asymptotic settings, as well as their applicability to geophysical systems, remain open questions.

A.3 Transition Rayleigh number (Ra_T) predictions

An empirical prediction for the columnar-to-plume transition is given by $Ra_{CP} \sim 5.4E^{-1.47}$, derived from laboratory and numerical $E = 10^{-4}$ to $E = 3 \times 10^{-8}$ rotating convection data in (Cheng *et al.* 2015). It was determined by finding the intersection between the best-fit trend for the rotationally-controlled, steep Nu–Ra scaling cases and the best-fit trend for nonrotating convection cases. Visualisations of the flow field in (Cheng *et al.* 2015) and thermal measurements in (King and Aurnou 2012) indicate that the breakdown of columnar structures into plume-like structures coincides with this intersection. Nieves *et al.* (2014) investigate regime transitions in asymptotically-reduced simulations. By analysing spatial autocorrelations and cross-correlations of temperature fluctuations, they find that the radial profiles of coherent flow structures undergo significant changes at $Ra \sim 55E^{-4/3}$, reflecting a transition from columns to plumes. For the parameter ranges explorable by NoMag and TROCONVEX, the Cheng *et al.* (2015) and Nieves *et al.* (2014) Ra_{CP} predictions occur in close proximity.

Though no specific predictions exist for Ra_{PGT}, in the asymptotically-reduced cases of (Julien *et al.* 2012a), the heat transfer diverges from the geostrophic turbulence scaling $\alpha = 3/2$ when $Ra \lesssim$

$3Ra_s$. Ecke and Niemela (2014) use this lower bound on the GT-scaling heat transfer as a broad estimate for $Ra_{_{PGT}}$ in $Pr > 3$ fluids.

Julien *et al.* (2012a) predict that $Ra_{_{GTU}} \sim E^{-8/5}Pr^{3/5}$, where geostrophic balance in the thermal boundary layer breaks down in the asymptotic equations. Ecke and Niemela (2014) find separate predictions for $Ra_{_{GTU}}$ depending on Pr: for $Pr = 0.7$ they argue that $Ra_{_{GTU}} \sim 1.3E^{-1.65}$ while for $Pr = 6$ they argue that $Ra_{_{GTU}} \sim 0.25E^{-1.8}$. These empirical estimates assume that transitions take the form $Ra_T \sim E^{\chi}$ and are derived by determining the best-fit value of χ.

Gilman (1977) predicts that the transition to nonrotating-style convection, $Ra_{_{UNR}}$, occurs when the system-scale buoyancy and Coriolis timescales become similar, or when $Ro_C \sim 1 \Rightarrow Ra \sim E^{-2}Pr$ (cf. Ecke and Niemela 2014). This prediction has been found to adequately describe the breakdown of large-scale zonal flows in spherical shell rotating convection simulations with free-slip boundary conditions (Aurnou *et al.* 2007, Gastine *et al.* 2014) and the breakdown of the large-scale circulation in cylindrical rotating convection experiments (Kunnen *et al.* 2008). Weiss and Ahlers (2011) also find transitions in the heat transfer corresponding to constant Ro_C values, but with an additional dependence on the aspect ratio Γ. Gastine *et al.* (2016) empirically estimate $Ra_{_{UNR}} = 100E^{-12/7}$ based on their spherical shell rotating convection simulations with non-slip boundary conditions. In the vicinity of this Ra value, they find that all measurable quantities become indistinguishable from the nonrotating cases. Finally, Ecke and Niemela (2014) find that the heat transfer becomes indistinguishable from nonrotating-style convection at $Ro_C \sim 0.35$ for $Pr \approx 0.7$.

These transition arguments have been compiled in table 1. Notably, no predictions have been made for $Ra_{_{GTU}}$ and $Ra_{_{UNR}}$ values. Larger datasets of more extreme rotating convection cases are needed, both to establish the validity of existing predictions and to develop new predictions for presently unconstrained transitions.

A.4 Pr $\ll$ 1 *fluids*

Liquid metal rotating convection follows a different set of predictions than those given for water and gas due to thermal diffusion operating on a far shorter timescale than viscous diffusion (e.g. King and Aurnou 2013). Rotating convection onsets via oscillatory modes at

$$Ra_o \simeq 17.4\left(\frac{E}{Pr}\right)^{-4/3} \tag{A.4}$$

(Chandrasekhar 1961, Julien and Knobloch 1998). The horizontal scale of these oscillatory structures is set by the thermal diffusivity:

$$\ell_o \simeq c\left(\frac{E}{Pr}\right)^{1/3}, H = c\left(\frac{\kappa H}{2\Omega}\right)^{1/3} \tag{A.5}$$

(see again Chandrasekhar 1961, Julien and Knobloch 1998), where $c = 2.4$.

The flow structure width ratio is then given by

$$m = D/\ell = c^{-1}\left(\frac{E}{Pr}\right)^{-1/3}, \Gamma = c^{-1}\left(\frac{2\Omega D^3}{\kappa H}\right)^{1/3}. \tag{A.6}$$

Since the onset flow structures are significantly wider, we choose $m \geq 5$ as the minimum rotation rate condition for liquid metal experiments:

$$\Omega_{\min} = \frac{62.5c^3\kappa H}{D^3}, \quad E_{\max} = \left(\frac{D}{5cH}\right)^3 Pr. \tag{A.7}$$

Table A1 demonstrates the accessible ranges of ℓ, m, E, and Fr for the liquid gallium ($Pr \simeq 0.025$) experiment RoMag. The $Fr \leq 0.1$ condition allows for a minimum accessible E of 2×10^{-7}, nearly an order of magnitude lower than existing liquid metal rotating convection studies in a cylinder.

The onset of wall modes Ra_w, predicted by (4), occurs after oscillatory convection for $E \gtrsim 0.16Pr^4$ ($E \gtrsim 6.3 \times 10^{-8}$ for $Pr \simeq 0.025$). Stationary onset Ra_s occurs at still higher Ra values, following (3). However, prior to stationary onset, Aurnou *et al.* (2018) find that broad-band turbulence

Table A1. Rotation rate limits for the $H = 0.5$ m tank on RoMag liquid gallium experiment ($Pr \simeq 0.025$), and corresponding flow structure widths ℓ, flow structure width ratios m, Ekman numbers E and Froude numbers Fr.

Ω (rad/s)	ℓ (cm)	m	E	Fr
$\Omega^M_{\text{min}} = 0.04$	10	2.0	1.5×10^{-5}	1.7×10^{-5}
$\Omega_{\text{min}} = 0.70$	4.0	5.0	9.3×10^{-7}	4.9×10^{-3}
$\Omega_{\text{max}} = 3.1$	2.4	8.3	2.0×10^{-7}	0.10
$\Omega^M_{\text{max}} = 6.3$	1.9	10.4	1.0×10^{-7}	0.40

Notes: Mechanical limitations are given by Ω^M_{min} and Ω^M_{max} while the $m \geq 5$ and $Fr \leq 0.1$ conditions are given by Ω_{min} and Ω_{max}, respectively.

induced by wall and oscillatory modes has already manifested at $Ra_b \gtrsim 4Ra_o$ in their liquid gallium experiments.

Liquid metals also behave differently from moderate Pr fluids under nonrotating convection. At $Ra \gtrsim 2 \times 10^9$, Cioni *et al.* (1987) find a $Nu \sim Ra^{2/7}$ scaling, consistent with $Pr \gtrsim 1$ results albeit with a different constant prefactor (Scheel and Schumacher 2016). At lower Rayleigh numbers ($\lesssim 5 \times 10^8$), though, studies find an $\alpha_{NR} \simeq 1/4$ scaling where the heat transfer is controlled by inertially driven, container-scale flows in the bulk rather than by viscous boundary layer processes (e.g. Jones *et al.* 1976, Cioni *et al.* 1987, Horanyi *et al.* 1999, King and Aurnou 2013, Schumacher *et al.* 2015). King and Aurnou (2013) find that their liquid gallium rotating convection cases conform to this nonrotating scaling for $Ra_{UNR} \simeq (E^2/Pr)^{-1}$, corresponding to $Ro_C \simeq \text{O}(1)$.

Figure A2 shows the behaviours accessible to the 0.5 m high tank on RoMag based on the above predictions. In contrast to higher Pr experiments, RoMag should be capable of delineating near-onset behaviours while encountering difficulty in accessing the nonrotating-style branch. RoMag should also be able to explore the transition to stationary convection for $E \gtrsim 3 \times 10^{-7}$.

While significant headway has been made in recent years towards understanding liquid metal rotating convection, open questions still abound with regard to the behaviours at $E \lesssim 10^{-6}$ and $Ra \gtrsim 10^7$. The $Pr \ll 1$ problem is generally relevant to a variety of planetary settings: in the outer cores of Mercury and the Earth and the metallic hydrogen layers of Jupiter and Saturn, Pr values are estimated to be $\lesssim 10^{-1}$ (Schubert and Soderlund 2011). Further studies at even more extreme conditions in liquid metal may be essential for understanding such systems.

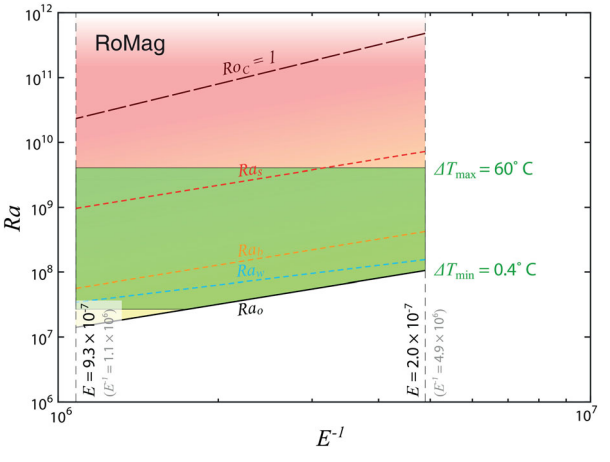

Figure A2. Rayleigh number Ra, plotted versus Ekman number, E, for the highest available tank size in the RoMag rotating convection experiment. The green box shows the range of accessible Ra–E space, assuming fixed fluid properties. The onset occurs with oscillatory convection at Ra_o, with predicted regime transitions indicated by dashed lines. (colour online).